Hindawi
Geofluids
Volume 2018, Article ID 7549831, 9 pages
https://doi.org/10.1155/2018/7549831

WILEY | Hindawi

Research Article

Microscopic Flow Characteristics of Fluids in Porous Medium and Its Relationship with Remaining Oil Distribution: A Case Study in Saertu Oilfield of Daqing in China

Z. Li,[1,2] X. Sun,[3] F. Wang,[4] and Y. Liang[5,6]

[1]*School of Marine Sciences, Sun Yat-sen University, Guangzhou 510006, China*
[2]*Key Laboratory of Offshore Oil Exploration and Development of Guangdong Higher Education Institutes, Guangzhou 510006, China*
[3]*Research Institute of Unconventional Oil & Gas, Northeast Petroleum University, Daqing 163318, China*
[4]*Exploration and Development Research Institute, Daqing Oilfield, Daqing 163453, China*
[5]*Key Lab of Minerals and Mineralization, Guangzhou Institute of Geochemistry, Chinese Academy of Sciences, Guangzhou 510640, China*
[6]*University of Chinese Academy of Sciences, Beijing 100049, China*

Correspondence should be addressed to X. Sun; sunxianda@petrochina.com.cn

Received 21 August 2017; Accepted 31 December 2017; Published 17 April 2018

Academic Editor: Stefano Lo Russo

The Saertu Oilfield of Daqing in northeast China has entered ultrahigh water-cut stage of development. Numerical simulation is applied in this paper to study characteristics of microscopic fluid velocity and flow pressures variation in the core pores in the Beier Area of Saertu Oilfield. The relationship between the remaining oil distribution and microscopic flow characteristics of fluid in the pores has been analyzed. Study results show that, in the reservoir with stronger heterogeneity of grain size and throat (corresponding to high coordinate number), high flow velocities tend to occur in relatively wider pore throats with great differentiation of flow velocities. The dominant passages are developed in high capacity channel, the detour flows are created in large porous channels, and the isolated islands are formed in small porous channels. The flow velocity declines slowly with long duration of high pressure. Few pores are swept by injected fluids with low sweep efficiency. The microscopic remaining oil is mainly distributed in cluster state. The content of remaining oil is higher with lower oil displacement efficiency. By contrast, in the reservoir with weaker heterogeneity of grain size and throat (corresponding to low coordinate number), high flow velocities also develop in relatively narrower pore throats with little differentiation of flow velocities. The development of detour flows is weaker in large porous channels. The flow velocity declines quickly with a short duration of high pressure. More pores are swept by fluids with high sweep efficiency. The remaining oil is mainly distributed in state of thin film on pore surface. The content of remaining oil is lower with higher oil displacement efficiency.

1. Introduction

The Saertu Oilfield of Daqing has entered ultrahigh water-cut stage of development. The remaining oil is highly dispersed in reservoirs with problems of low flooding efficiency and of severely ineffective cycles. The preliminary statistics indicate that the recoverable remaining oil reserve accounts for 40% of the total oil reserves but with difficulties in potential tapping [1–3]. Up to now, the main studies on the remaining oil have been focused on macroscopic distribution characteristics in the aspects of well pattern control, reservoir heterogeneity and sedimentary facies belts, and so forth [4–9]. When the comprehensive water cut of an oilfield reaches an ultrahigh stage, macroscopic study cannot well solve the problems of remaining oil distribution, so a more detailed investigation in a pore scale is necessary [10–14]. Previous studies indicated that the distribution of microscopic remaining oil in reservoirs was associated with pore structure and fluid

flow in pores [15–22]. A combined study on distribution characteristics of the microscopic remaining oil in reservoirs on a comprehensive basis of pore structures, heterogeneity, and microscopic flow of fluid in pores is significant to make reasonable development plans during the ultrahigh water-cut stage. Based on the pore structure characteristics in the reservoirs of the Beier Area in Saertu oilfield, the images of casting thin sections of core samples are selected to extract the pores and characterize boundaries. Then the geological models and mathematical models of a pore scale are established to simulate the fluid velocity and flow pressure distribution in pores with different pore structures, with aims of understanding the relationship between the velocity field of fluid in pores and distribution of microscopic remaining oil and of analyzing the oil displacement efficiency as well.

2. Geological Features of the Beier Area of Saertu Oilfield

The Beier Area of Saertu Oilfield is located in the northern part of Daqing Placanticline from the Songliao Basin (Figure 1) with a gentle structure and formation dip angle of about 3° [23]. There are many NNE-trending normal faults in this block. The maximum of the extensional fault can be up to 6.6 km in length with a minimum length of 0.5 km. The maximum of fault throw can be up to 92.0 m with a minimum fault throw of 1.2 m, with an average fault dip angle of about 52°.

Three sets of major reservoir formations were developed in the Beier Area of Saertu Oilfield, which are termed as the Saertu, Putaohua, and Gaotaizi Formations (Figure 2). The reservoirs consist of large-scale fluviodeltaic sedimentary sequences with a strong heterogeneity and a burial depth of 870~1200 m [24]. The main rock types include interbedded sandstone and mudstone. At present, the reservoirs of Saertu, Putaohua, and Gaotaizi are the main producing factories (reservoirs) in which Saertu reservoir is divided into three oil formations, the Putaohua into two, and the Gaotaizi into four.

The target layer of this study is the first segment of the Putaohua Formation (member PI). Member PI is favorable in permeability with an average thickness of 21.4 m. The lithology assemblage consists of sandstone and siltstone. The average air permeability is 0.649 μm^2 and the average porosity is 29.8% [25]. The core samples for this study are from the Putaohua Formation and the coring horizons are the second layer in member PI for Sample 1 and the seventh layer in member PI for Sample 2. Both samples are fine-grained oil-bearing sandstone.

3. Mathematical Model of Microscopic Flow of Fluid in Porous Medium

The reservoir is regarded as a porous medium composed of skeleton structures, which consist of solid materials and a large number of dense micropores separated by skeletons [26, 27]. If the porous medium is continuous, the flow of fluid in porous medium can be divided into four different scales, that is, the pore scale, core scale, mega scale, and giga scale [28, 29]. The fluid flow in pore throats of cores belongs to microscopic flow, which is also known as pore scale. The microscopic flow is affected by the heterogeneity of porous medium [30–34]. On the pore scale, the fluid flow is generally considered to be continuous. If the density and temperature of fluids in the pore are constant, the flow of fluids in the pore scale can be described using the Navier-Stokes equation [35–37].

The Navier-Stokes equation governs the flow of fluids [38–41], and it can be regarded as Newton's second law of fluid. For compressible Newtonian fluid, the Navier-Stokes equation is

$$\underbrace{\rho\left(\partial u/\partial t + u\cdot\nabla u\right)}_{1} = \underbrace{-\nabla pI}_{2} + \underbrace{\nabla\cdot\left(\eta\left(\nabla u + (\nabla u)^{T}\right) - (2/3)\,\eta\,(\nabla\cdot u)\,I\right)}_{3} + \underbrace{F}_{4}, \quad (1)$$

where u is the fluid velocity (m/s), p is the fluid pressure (Pa), ρ is the fluid density (kg/m^3), η is the fluid dynamic viscosity (kg/(m·s)), and I is the unit matrix. In the equation, term (1) is for inertia force, term (2) is for pressure, term (3) is for viscous force, and term (4) is for external force acting on the fluid.

The Navier-Stokes equation and the continuity equation must be solved simultaneously. The continuity equation is

$$\frac{\partial\rho}{\partial t} + \nabla\cdot(\rho u) = 0. \quad (2)$$

The Navier-Stokes equation for momentum conservation and the continuity equation for mass conservation are the kernel of mathematical model of fluid flow, which describe the motion law of viscous fluid. It is nonlinear partial differential equation that is very difficult and complex to solve, but it can be simplified to get the approximate solution in some conditions. When the Reynolds number is very low ($Re \ll 1$), the inertial force (time-dependent inertial force) is very small compared to the viscous force, and it is neglected in solving the Navier-Stokes equation. External force term (4) might be neglected for without consideration of gravity.

For the incompressible fluids (the density of fluids is constant), the continuity equation is

$$\nabla\cdot u = 0. \quad (3)$$

As the divergence of velocity is zero, there is

$$-\frac{2}{3}\eta\,(\nabla\cdot u)\,I = 0. \quad (4)$$

Therefore, the Navier-Stokes equation can be simplified as

$$\rho\,(u\cdot\nabla u) = \nabla\cdot\left[-pI + \eta\left(\nabla u + (\nabla u)^{T}\right)\right]. \quad (5)$$

The Navier-Stokes equation, the continuity equation, relative variables, and definite conditions constitute the mathematical model of microscopic flow of fluid in porous medium.

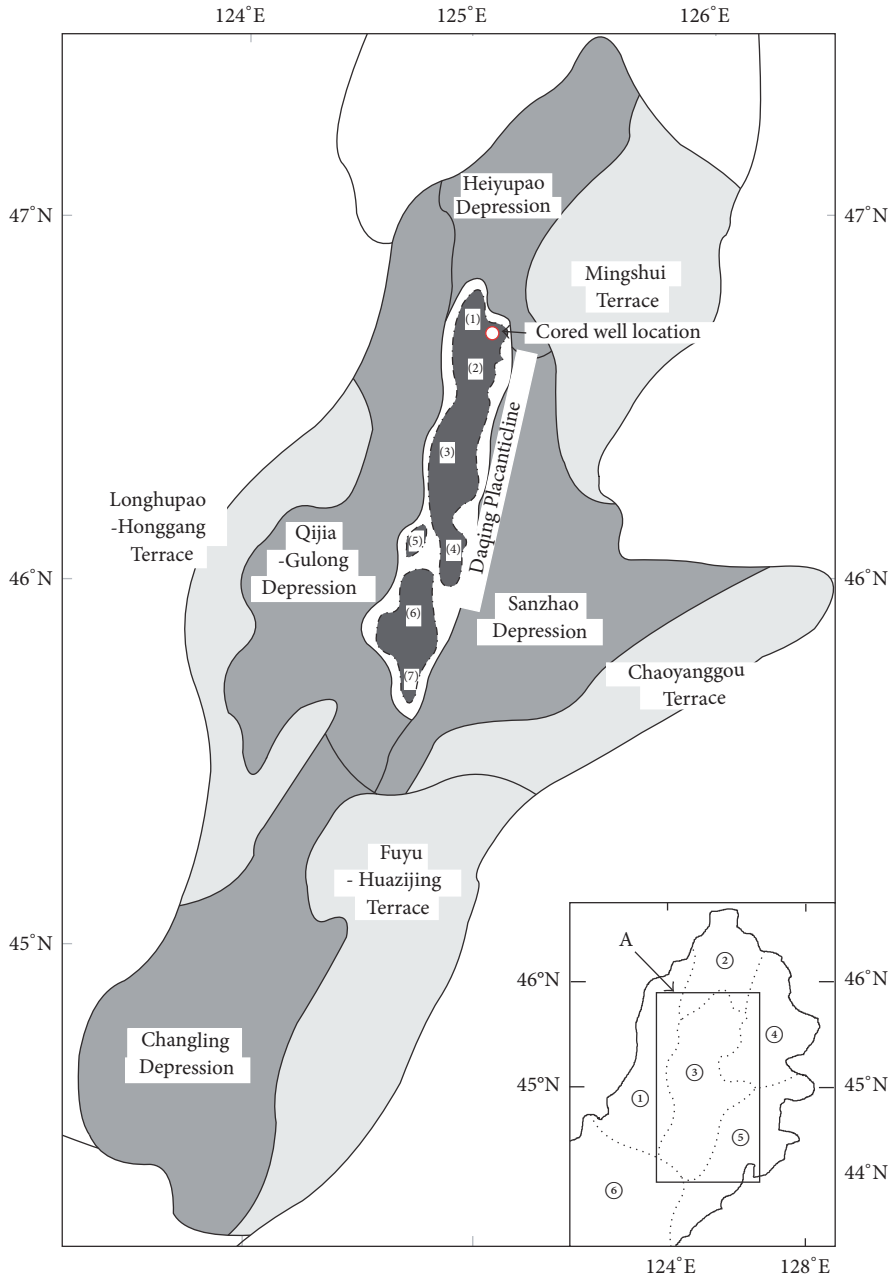

Figure 1: Structural outline map of the central depression zone: A-Location of the central depression zone in the Songliao Basin, ① the western slope zone, ② the northern plunge zone, ③ the central depression zone, ④ the northeastern uplift zone, ⑤ the southeastern uplift zone, and ⑥ the southwestern uplift zone.

4. Numerical Modeling Process

4.1. The Building of the Geological Model. Two core samples (Sample 1 and Sample 2) with different pore structures from the Putaohua Formation in the Beier Area of the Saertu Oilfield were collected to be studied in this paper. Parameters that characterize the pore structures include channel radius, coordinate number, pore throat ratio, and heterogeneity coefficient, among which the coordinate number refers to the number that a pore links to throat. Grains and throat distribution of Sample 1 show stronger heterogeneity with an average coordinate number of 4.5. Grains and throat

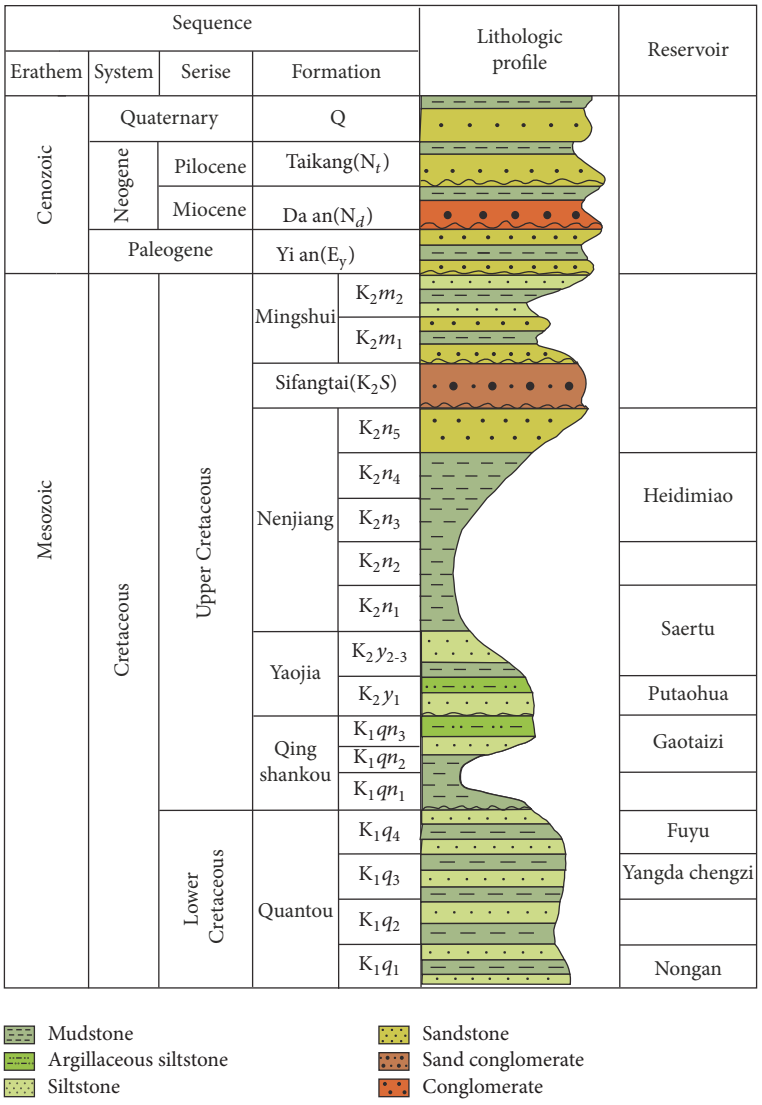

Figure 2: Profile map of the different layers in Beier area.

distribution of Sample 2 show weaker heterogeneity with an average coordinate number of 2.5. Geological model is designed on the basis of the images of casting thin sections of the core samples (Figures 3 and 4); that is, casting images are transformed into geometric model by pore extracting and boundary characterizing [42–45]. The dimensions of geological models of Sample 1 and Sample 2 are both 1657 μm $\times$ 1228 μm and parameters of the pore structures in the model are listed in Table 1. Fluid flow in pores of model is laminar with a flow direction from right to left and without fluid entering grains.

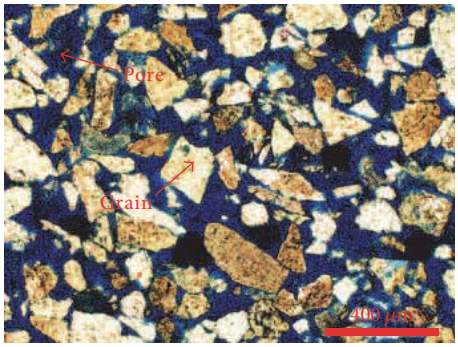

Figure 3: Image of cast Sample 1.

4.2. Model Parameters and Boundary Conditions. The fluid parameters and boundary condition settings of the models are listed in Tables 2 and 3, respectively. The left boundary is the outlet and the right boundary is the inlet, with the upper and lower boundaries as symmetrical boundaries. The flow is symmetric and there is on axial velocity on the symmetric plane about the upper and lower boundaries. There are no fluid flowing and no grain slipping at the grain boundaries.

Table 1: Parameters of pore structure in the geological models.

Number	Average pore diameter (μm)	Average coordinate number	Average pore throat ratio	Minimum of throat (μm)	Maximum of throat (μm)	Average of throat (μm)	Heterogeneity coefficient
(1)	149.21	4.5	4.03	1.29	154.55	35.96	0.56
(2)	136.17	2.5	4.55	4.65	101.98	25.31	0.49

Table 2: Model parameters.

Variables	Value	Description
ρ	1000 kg/m^3	Fluid density
η	0.0015 kg/(m·s)	Dynamic viscosity
p	0.75 Pa	Pressure drop

Table 3: Boundary condition settings.

Boundary type	Boundary setting	Value
Outlet	Outlet, pressure	0
Inlet	Inlet, pressure	0.75 Pa
Grain boundaries	Wall, no fluid flowing, and no grain slipping	-
Symmetry boundaries	Symmetry, on axial fluid flowing	-

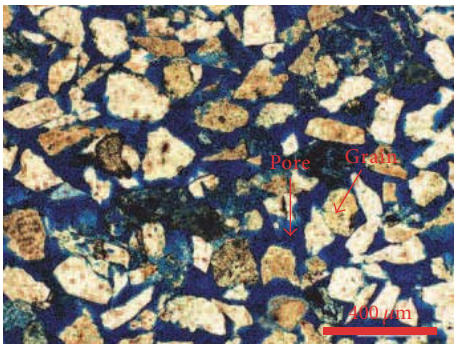

Figure 4: Image of cast Sample 2.

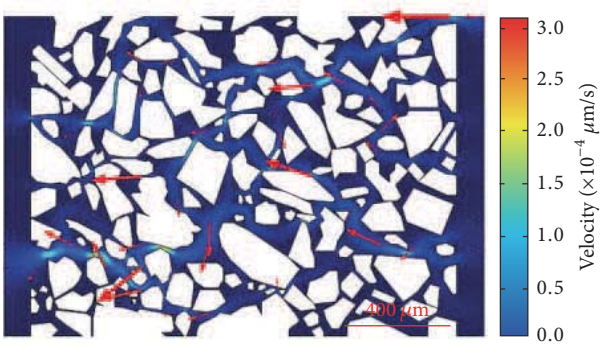

Figure 5: Simulation results of pore velocity field of Sample 1 (μm/s).

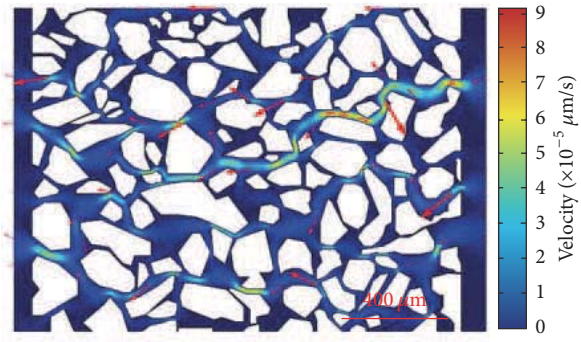

Figure 6: Simulation results of pore velocity field of Sample 2 (μm/s).

4.3. Simulation Process. COMSOL Multiphysics is applied to simulate the microscopic flow characteristics of fluid in the pore throats of core samples with different pore structures (different coordinate numbers). Core Sample 1 and Sample 2 are, respectively, simulated to unravel the distribution characteristics of fluid velocity and pressure and their relationship with remaining oil in the pores, with only changed parameters of pore structures in the geological models.

5. Analyses of Simulation Results

5.1. Characteristics of Fluid Velocity Field in Core Pores and Their Relationship with Distribution of Remaining Oil. Figures 5 and 6 show the simulating images of velocity field distribution of fluids in the pores of core Sample 1 and Sample 2, respectively. Figure 7 shows the types of microscopic remaining oil in the PI of the Beier area based on analytical technology of fluorescent microscope with frozen sectioning [46–49]. According to Figure 5, the grain size and the throat of Sample 1 have stronger heterogeneity (with coordinate number of 4.5). The high flow velocities tend to occur in the relatively wider pore throats with great differentiation of flow velocities. The dominant passages are developed in high capacity channels and the detour flows are created in large porous channels. The isolated islands are formed in small porous channels because of the insufficient driving force of fluids. Due to the low fluid velocity and inefficient sweep of fluids, the remaining oil of cluster state is produced (Figure 7(a)). In particular, the other remaining oil of cant state is formed in corners of complicated space of pores (Figure 7(b)). The main composition of clay minerals in the core samples is kaolinite. The flaky crystal aggregate

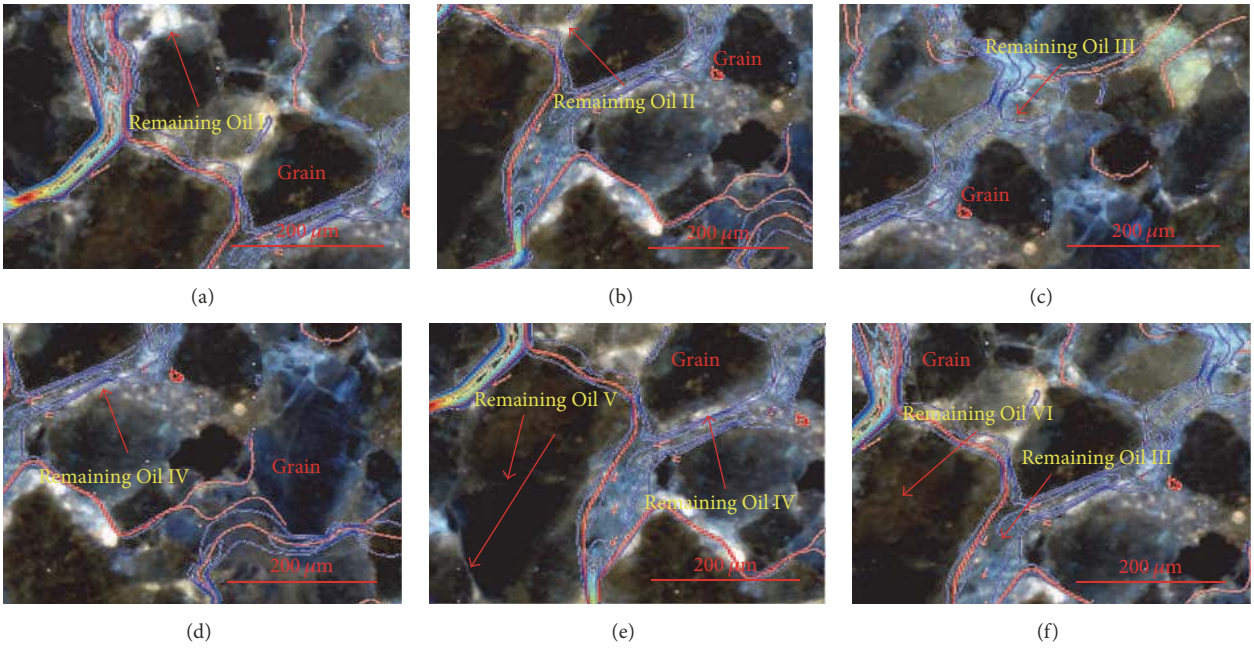

Figure 7: Types of microscopic remaining oil: the red line represented the high flow velocities and the blue line represented the low flow velocities. (a) Remaining Oil I: remaining oil of cluster state, (b) Remaining Oil II: remaining oil of cant state, (c) Remaining Oil III: remaining oil of intergranular adsorbing state, (d) Remaining Oil IV: remaining oil of state of thin film on pore surface, (e) Remaining Oil V: remaining oil of slit state, (f) Remaining Oil VI: remaining oil of particle adsorbing state.

of kaolinite in large pore throat has undergone long-term mechanical flushing from fluids, which breaks down the crystal framework of aggregate into fine particles [50]. The particles in the pore fluid are mixed with oil and concentrated locally to form the remaining oil of intergranular adsorbing state (Figure 7(c)). In addition, since the particle surfaces in large pore throat has an absorption effect on oil, the flushing in dominant passages cannot displace this type of absorbed residual oil. In such a case, the remaining oil of state of thin film on pore surface is formed (Figure 7(d)). In some pores with small diameter on the surface of mineral particle, the remaining oil of particle adsorbing state is produced because oil in micropores on the surface of mineral particle cannot be displaced under the effect of capillary force (Figure 7(f)).

As shown in Figure 6, the grain size and throat in Sample 2 are of weaker heterogeneity (with coordinate number of 2.5), and the high flow velocities also develop in the relatively narrower throat with less differentiation of flow velocities. The degree of detour flow is lower in large porous channels. The effective sweep degree of fluid in small pore throat is higher. As a result, the remaining oil in different states, such as in cluster state (Figure 7(a)), cant state (Figure 7(b)), intergranular adsorbing state (Figure 7(c)), and state of thin film on pore surface (Figure 7(d)) can be produced. However, due to flushing effects by the high velocity fluids, the relative contents of the remaining oil of cluster state and remaining oil of intergranular adsorption in Sample 2 are lower than those in Sample 1, whereas the relative content of the remaining oil of state of thin film on pore surface in Sample 2 is higher than that in Sample 1 (Table 4). On the other hand, small connective crevices among particles are formed because of the development of mineral dissolved fissures, cracks of mineral particles, and cleavage cracks. Because oil in the crevices is suffered holding force by effects of capillary force, it cannot be displaced by the flowing fluids to form the remaining oil of slit state (Figure 7(e)). In addition, the remaining oil of particle adsorbing state is formed in response to the effect of capillary force (Figure 7(f)).

5.2. Microscopic Flow Characteristics of Fluid in Core Pores and Their Relationship with Displacement Efficiency. Figures 8 and 9 show the simulation images of fluid pressure variations in pores of Sample 1 and Sample 2, respectively. According to Figure 8, the high flow velocities of Sample 1 concentrate mainly in relatively wider throats. The flow velocity declines slowly with slight variations of flow pressure and a long duration of high pressure. Few pores are swept by fluids with a low degree of flushing. The content of remaining oil in free state is high, whereas it is low for the remaining oil in bound state. The content of movable remaining oil (movable remaining oil refers to the remaining oil that can be exploited under the current technological level and exploitation conditions) is relatively high but the oil displacement efficiency is low (Table 5). As shown in Figure 9, the high flow velocities of Sample 2 concentrate mainly in the relatively narrower throats. The flow velocity declines quickly with great variations of flow pressure and a shorter duration of high pressure as well. More pores are swept by fluids with a higher degree of flushing. Compared with that of Sample 1, the content of the remaining oil in bound state is higher but

Table 4: Types and relative contents of the microscopic remaining oil.

Sample number	Horizon	State of thin film on pore surface (%)	Slit state (%)	Cant state (%)	Cluster state (%)	Particle adsorbing state (%)	Intergranular adsorbing state (%)
(1)	PI_2	15.54	0.00	1.36	44.09	2.45	36.56
(2)	PI_7	30.96	3.42	1.79	28.49	5.51	29.82

Table 5: The remaining oil distribution and displacement efficiency in different microscopic flow field.

Sample number	Horizon	Bound state remaining oil (%)	Semibound state remaining oil (%)	Free state remaining oil (%)	Movable remaining oil (%)	Water cut (%)	Flushing degree
(1)	PI_2	17.99	1.36	80.65	36.89	7	Low
(2)	PI_7	39.89	1.79	58.31	3.54	76	High

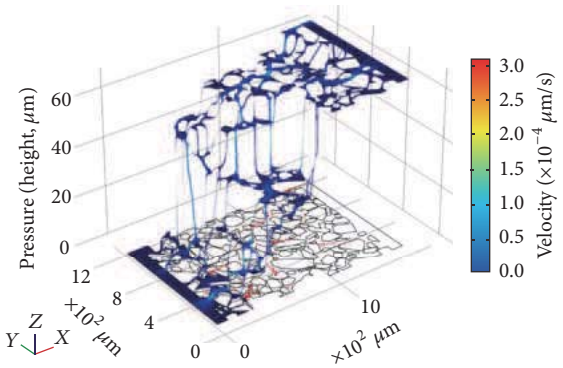

Figure 8: Simulation results of pore pressure decline of Sample 1.

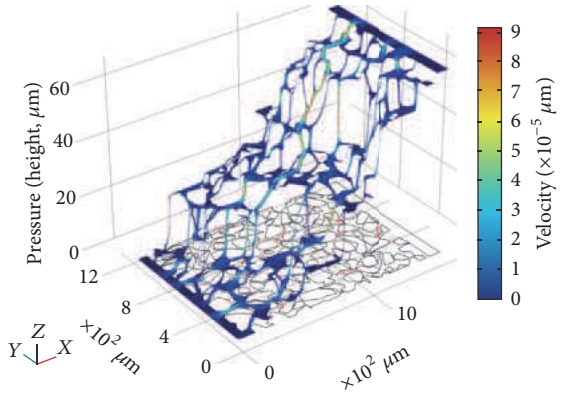

Figure 9: Simulation results of pore pressure decline of Sample 2.

it is lower for the remaining oil in free state. The content of movable remaining oil is lower with higher oil displacement efficiency (Table 5).

In Table 5, bound state refers to the remaining oil which is adsorbed on the particle surface, including state of thin film on pore surface, particle adsorbing, and slit; semibound state refers to the remaining oil which is in the outer layer of bound state or far from pore surface, including cant state. Free state refers to the remaining oil which is retained far from pore surface, including cluster state and intergranular adsorbing state.

6. Conclusions

(1) The microscopic flow characteristics of fluid in core pores are closely related to the pore structures and heterogeneity of throat. In the core with stronger heterogeneity of both grain size and throat, the high flow velocities tend to occur in the relatively wider throats with great differentiation of flow velocities. The dominant passages are developed in high capacity channels and the detour flows are created in large porous channels. By contrast, the isolated islands are formed in small porous channels. The flow velocity declines slowly with slight variations of flow pressure and a long duration of high pressure. The efficient sweep area is small with a low degree of flushing.

(2) In the core with weaker heterogeneity of both grain size and throat, the high flow velocities also develop in the relatively narrower throats with little differentiation of flow velocities. The development of detour flows is weaker in large porous channels. The flow velocity declines quickly with greater variations of flow pressure and a shorter duration of high pressure. The efficient sweep area is larger with a higher degree of flushing.

(3) The microscopic flow characteristics of fluid in core pores have a significant influence on the distribution and formation of the remaining oil. In the core with stronger heterogeneity of grain size and throat, the microscopic remaining oil is mainly distributed in cluster state by microscopic fingering of fluids flow and detour flows. The content of the remaining oil is larger with lower oil displacement efficiency.

(4) In the core with weaker heterogeneity of grain size and throat, the remaining oil is mainly distributed in microscopic water flooded area in state of thin film on pore surface. The content of the remaining oil is lower with higher oil displacement efficiency.

Conflicts of Interest

The authors declare that they have no conflicts of interest.

Acknowledgments

This study was supported by the National Science and Technology Major Project (Grant no. 2016ZX05054013). The authors are grateful to Dr. Ge Lin and Feng Guo for their careful reviews, comments, suggestions.

References

[1] D. K. Han, "Status and challenges for oil and gas field development in China and directions for the development of corresponding technologies," *International Journal of Engineering Science*, vol. 12, pp. 51–57, 2010.

[2] C. L. Shi, F. H. Zhang, and P. Chen, "Affection of Simulating Water-flooding by Water Injection Tests on Reservoir Properties," *Journal of Southwest Petroleum University. Science & Technology Edition*, vol. 35, pp. 87–93, 2013.

[3] W. C. Yan and J. M. Sun, "Analysis of research present situation of microscopic remaining oil," *Progress in Geophysiscs*, vol. 31, pp. 2198–2211, 2016.

[4] H. Wei, S. Shi, P. Zhao, D. Huo, and W. Zhu, "Research on residual oil distribution regular with the application of facies controlled modeling and reservoir numerical simulation," *Advanced Materials Research*, vol. 616-618, pp. 126–132, 2013.

[5] P. Yang, H. Guo, and D. Yang, "Determination of residual oil distribution during waterflooding in tight oil formations with NMR relaxometry measurements," *Energy & Fuels*, vol. 27, no. 10, pp. 5750–5756, 2013.

[6] C. Feng, Z. Bao, L. Yang, X. Si, G. Xu, and X. Han, "Reservoir architecture and remaining oil distribution of deltaic front underwater distributary channel," *Petroleum Exploration and Development*, vol. 41, no. 3, pp. 358–364, 2014.

[7] T. B. N. Nguyen, T. Q. C. Dang, Z. Chen, and L. X. Nghiem, "Effects of lithofacies and reservoir heterogeneity on improved oil recovery processes," in *Proceedings of the SPE Canada Heavy Oil Technical Conference 2015, CHOC 2015*, pp. 217–233, can, June 2015.

[8] E. W. Al-Shalabi and B. Ghosh, "Effect of pore-scale heterogeneity and capillary-viscous fingering on commingled water-14.flood oil recovery in stratified porous media," *Journal of Petroleum Engineering*, pp. 1–14, 2016.

[9] H. Wei, H. Zhu, S. Shi et al., "Study of distribution of remaining oil in west block of the third district in North Saertu," *Earth Sciences Research Journal*, vol. 20, no. 2, pp. A1–A4, 2016.

[10] E. V. Lebedeva and A. Fogden, "Micro-CT and wettability analysis of oil recovery from sand packs and the effect of waterflood salinity and kaolinite," *Energy & Fuels*, vol. 25, no. 12, pp. 5683–5694, 2011.

[11] S. W. Pan, H. J. Liang, L. Li, H. N. Luo, and J. H. Wang, "Research progress on simulation of microscopic remaining oil," *Lithologic Reservoirs*, vol. 25, pp. 16–20, 2013.

[12] W. Daigang, H. Yongle, and S. Jingjing, "X-ray MCT based numerical analysis of residual oil pore-scale characteristics under various displacing systems," *Journal of Petroleum Science and Engineering*, vol. 135, pp. 168–176, 2015.

[13] Q. Xie, J. M. Wang, and S. B. Shi, "Research on heterogeneity of Chang 2 reservoir in Taiyangwan area, Ordos Basin," *Lithologic Reservoirs*, vol. 27, pp. 61–67, 2015.

[14] B. Y. Ma and S. Y. Xu, "Overview on research methods of microcosmic remaining oil distribution," *Zhongzhou Coal*, vol. 251, pp. 142–150, 2016.

[15] Y. F. Wang and Y. Bao, "Relationship between reservoir pore structure and displacement efficiency," *Henan Petroleum*, vol. 13, pp. 23–60, 1999.

[16] G. Y. Huang and Z. H. Wang, "Simulation experiment of water flooding core for regularity of remaining oil microcosmic distribution," *Neijiang Science and Technology*, vol. 13, pp. 155–160, 2006.

[17] T. B. Sun, C. Y. Lin, S. T. Cui, S. Z. Zhang, P. Wang, and L. Wang, "Microscopic heterogeneity characteristics of marine clastic reservoirs and effect to remaining oil distribution in high water cut stage," *Journal of Central South University of Science and Technology*, vol. 44, pp. 3282–3292, 2013.

[18] Y. Zhang and X. Li, "The influence of microscopic pore structure on microscopic residual oil in sandstone reservoir," *Advanced Materials Research*, vol. 787, pp. 721–725, 2013.

[19] A. Rodríguez de Castro, M. Oostrom, and N. Shokri, "Effects of shear-thinning fluids on residual oil formation in microfluidic pore networks," *Journal of Colloid and Interface Science*, vol. 472, pp. 34–43, 2016.

[20] Y. G. Guo, "Relationship between pore-throat structure and remaining oil distribution in extra -low permeability reservoir," *Fault-Block Oil & Gas Field*, vol. 24, pp. 218–221, 2017.

[21] J. Li, H. Jiang, C. Wang et al., "Pore-scale investigation of microscopic remaining oil variation characteristics in water-wet sandstone using CT scanning," *Journal of Natural Gas Science and Engineering*, vol. 48, pp. 36–45, 2017.

[22] P. Xiao, X. Leng, H. Xiao et al., "Investigation effect of wettability and heterogeneity in water flooding and on microscopic residual oil distribution in tight sandstone cores with NMR technique," *Open Physics*, vol. 15, no. 1, pp. 544–550, 2017.

[23] J. L. Yang, "Development characteristics of structure and petroleum accumulation in the Songliao basin," *China. Journal of Changchun University of Earth Sciences*, vol. 9, pp. 9–20, 1983.

[24] J. Sui, H. Q. Zhao, and X. G. Lv, *Study of large fluvial-delta depositional reservoir of Daqing oilfield*, Petroleum Industry Press, Beijing, China, 2000.

[25] Y. L. Jiao, "Depositional pattern of the Class II oil reservoir in the North of Sa'ertu development area of Daqing oil field," *Journal of Daqing Petroleum Institute*, vol. 34, pp. 19–22, 2010.

[26] S. M. Shah, J. P. Crawshaw, and E. S. Boek, "Preparation of microporous rock samples for confocal laser scanning microscopy," *Petroleum Geoscience*, vol. 20, no. 4, pp. 369–374, 2014.

[27] S. M. Shah, J. P. Crawshaw, and E. S. Boek, "Three-dimensional imaging of porous media using confocal laser scanning microscopy," *Journal of Microscopy*, vol. 265, no. 2, pp. 261–271, 2017.

[28] X. Ge, Y. Fan, J. Li, and M. Aleem Zahid, "Pore structure characterization and classification using multifractal theory-an application in santanghu basin of western china," *Journal of Petroleum Science and Engineering*, vol. 127, pp. 297–304, 2015.

[29] L. Xiao, C.-C. Zou, Z.-Q. Mao et al., "An empirical approach of evaluating tight sandstone reservoir pore structure in the absence of NMR logs," *Journal of Petroleum Science and Engineering*, vol. 137, pp. 227–239, 2016.

[30] Y. Zaretskiy, S. Geiger, K. Sorbie, and M. Förster, "Efficient flow and transport simulations in reconstructed 3D pore geometries," *Advances in Water Resources*, vol. 33, no. 12, pp. 1508–1516, 2010.

[31] S. Geiger, K. S. Schmid, and Y. Zaretskiy, "Mathematical analysis and numerical simulation of multi-phase multi-component flow in heterogeneous porous media," *Current Opinion in Colloid & Interface Science* , vol. 17, no. 3, pp. 147–155, 2012.

[32] L. J. Zhao, Q. S. Li, and X. S. Wang, "Analysing for flow field of water displacing oil in microscopic pore," *Advanced Materials Research*, vol. 774-776, pp. 267–270, 2013.

[33] Y. Ma, W. Li, and C. Liu, "Microscopic characteristics of water flooding and the affecting factors of low-permeability sandstone reservoir in Zhidan area, Ordos Basin, China," *Energy Exploration & Exploitation*, vol. 33, no. 2, pp. 145–156, 2015.

[34] B. P. Muljadi, M. J. Blunt, A. Q. Raeini, and B. Bijeljic, "The impact of porous media heterogeneity on non-Darcy flow behaviour from pore-scale simulation," *Advances in Water Resources*, vol. 95, pp. 329–340, 2016.

[35] J. Bear, *Dynamics of Fluids in Porous Media*, Dover publications, INC, New York, NY, USA, 1972.

[36] S. Sirivithayapakorn and A. Keller, "Transport of colloids in saturated porous media: A pore-scale observation of the size exclusion effect and colloid acceleration," *Water Resources Research*, vol. 39, no. 4, pp. SBH111–SBH1111, 2003.

[37] M. Auset and A. A. Keller, "Pore-scale processes that control dispersion of colloids in saturated porous media," *Water Resources Research*, vol. 40, no. 3, pp. W035031–W0350311, 2004.

[38] M. Sajben, J. C. Kroutil, and C. P. Chen, "A High-Speed Schlieren Investigation of Diffuser Flows with Dynamic Distortion," in *In 13th Propulsion Conference*, p. 875, 1977.

[39] T. J. Bogar, M. Sajben, and J. C. Kroutil, "Characteristic frequencies of transonic diffuser flow oscillations," *AIAA Journal*, vol. 21, no. 9, pp. 1232–1240, 1983.

[40] J. T. Salmon, T. J. Bogar, and M. Sajben, "Laser Doppler velocimeter measurements in unsteady, separated, transonic diffuser flows," *AIAA Journal*, vol. 21, no. 12, pp. 1690–1697, 1983.

[41] T. Hsieh, A. B. Wardlaw, P. Collins, and T. Coakley, "Numerical investigation of unsteady inlet flowfields," *AIAA Journal*, vol. 25, no. 1, pp. 75–81, 1987.

[42] A. S. Al-Kharusi and M. J. Blunt, "Network extraction from sandstone and carbonate pore space images," *Journal of Petroleum Science and Engineering*, vol. 56, no. 4, pp. 219–231, 2007.

[43] Z. Jiang, K. Wu, G. Couples, M. I. J. Van Dijke, K. S. Sorbie, and J. Ma, "Efficient extraction of networks from three-dimensional porous media," *Water Resources Research*, vol. 43, no. 12, Article ID W12S03, 2007.

[44] H. Dong and M. J. Blunt, "Pore-network extraction from micro-computerized-tomography images," *Physical Review E: Statistical, Nonlinear, and Soft Matter Physics*, vol. 80, no. 3, Article ID 036307, 2009.

[45] M. J. Blunt, B. Bijeljic, H. Dong et al., "Pore-scale imaging and modelling," *Advances in Water Resources*, vol. 51, pp. 197–216, 2013.

[46] X. D. Sun, L. M. Suo, and H. Q. Jiang, "Laser scanning confocal microscope in micropores study," *Journal of Chinese Electronic Microscopy Society*, vol. 23, pp. 517-518, 2004.

[47] K. P. Song, S. J. Li, W. Fang, J. W. Wu, and W. Z. Mu, "Fluorescence analysis on changeable rules of microscopic remaining oil after polymer flooding," *Acta Petrolei Sinica*, vol. 26, pp. 92–95, 2005.

[48] Y. Li, J. Li, S. Ding, and X. Sun, "Characterization of Remaining Oil After Polymer Flooding by Laser Scanning Confocal Fluorescence Microscopy," *Journal of Dispersion Science and Technology*, vol. 35, no. 7, pp. 898–906, 2014.

[49] Y. Li, Y. Yang, X. Sun et al., "The application of laser confocal method in microscopic oil analysis," *Journal of Petroleum Science and Engineering*, vol. 120, pp. 52–60, 2014.

[50] H. L. Peng, X. P. Zhou, G. J. Yao, and L. T. Sun, "Laboratory research on microscopic distribution of residual oil after polymer driving and how to improve recovery factor for reservoirs with big porous channels," *Natural Gas Exploration Development*, vol. 28, pp. 62–65, 2005.